Research article

Ning Li, Ying Suet Lau, Yanqin Miao* and Furong Zhu*

# Electroluminescence and photo-response of inorganic halide perovskite bi-functional diodes

https://doi.org/10.1515/nanoph-2018-0149
Received September 14, 2018; revised November 3, 2018; accepted November 10, 2018

**Abstract:** In this work, we report our efforts to develop a novel inorganic halide perovskite-based bi-functional light-emitting and photo-detecting diode. The bi-functional diode is capable of emitting a uniform green light, with a peak wavelength of 520 nm, at a forward bias of >2 V, achieving a high luminance of >$10^3$ cd/$m^2$ at 7 V. It becomes an efficient photodetector when the bi-functional diode is operated at a reverse bias, exhibiting sensitivity over a broadband wavelength range from ultraviolet to visible light. The bi-functional diode possesses very fast transient electroluminescence (EL) and photo-response characteristics, e.g. with a short EL rising time of ~6 μS and a photo-response time of ~150 μS. In addition, the bi-functional diode also is sensitive to 520 nm, the wavelength of its peak EL emission. The ability of the bi-functional diodes for application in high speed visible light communication was analyzed and demonstrated using two identical bi-functional diodes, one performed as the signal generator and the other acted as a signal receiver. The dual functions of light emission and light detection capability, enabled by bi-functional diodes, are very attractive for different applications in under water communication and visible light telecommunications.

**Keywords:** halide perovskite; light-emitting diode; photo-detector; visible light communication.

## 1 Introduction

Bi-functional devices enabling light emission and photo detection in one configuration are attractive for various applications and valuable for simplifying fabrication processes and reducing the device size [1–5]. To obtain such bi-functionality, one strategy is to stack a photodiode (PD) and a light emitting diode (LED) together with an inter electrode between the two units [1, 2]. This includes a tedious control of the inter electrode and precise design of the multi-layer configuration. Another method is to employ a photo sensitive layer in the LEDs [3–5], where the energy levels of the interlayers should be well aligned and most of the materials are not solution processable.

In the past years, great progress has been made in both organic emitting materials and their light emitting diodes (OLEDs), but the bigger full width at half maximum (FWHM) for OLEDs make them unsuitable applied in photo detection field [6–8]. By contrast, perovskite materials are emerging as promising candidates in a variety of applications due to their excellent optoelectronic properties, such as high carrier mobility, large absorption coefficient and saturated light emission characteristics [9–16] for various applications in solar cells [9–12] and light emitting devices [13–16]. The inorganic halide perovskite, e.g. cesium lead bromide ($CsPbBr_3$), is known for its good thermal stability and excellent optoelectronic properties [16–24]. The $CsPbBr_3$ perovskite is intensively investigated for application in both solar cells [17–19] and LEDs [15, 20, 21] due to its simultaneously excellent light absorption and saturated light emission properties. In $CsPbBr_3$ based solar cells, efficiency up to 6.7% was achieved indicating $CsPbBr_3$ as an excellent light sensitive material [19]. Meanwhile, $CsPbBr_3$ also is suitable for photo detection applications with high sensitivity and responsivity [22–24]. On

***Corresponding authors: Yanqin Miao,** Department of Physics, Institute of Advanced Materials and Institute of Research and Continuing Education (Shenzhen), Hong Kong Baptist University, Kowloon Tong, Hong Kong, China; and Key Laboratory of Interface Science and Engineering in Advanced Materials of Ministry of Education and Research Center of Advanced Materials Science and Technology, Taiyuan University of Technology, Taiyuan 030024, China, e-mail: miaoyanqin@tyut.edu.cn. http://orcid.org/0000-0003-2659-7696; and **Furong Zhu,** Department of Physics, Institute of Advanced Materials and Institute of Research and Continuing Education (Shenzhen), Hong Kong Baptist University, Kowloon Tong, Hong Kong, China, e-mail: frzhu@hkbu.edu.hk
**Ning Li and Ying Suet Lau:** Department of Physics, Institute of Advanced Materials and Institute of Research and Continuing Education (Shenzhen), Hong Kong Baptist University, Kowloon Tong, Hong Kong, China

the other hand, with an exceptional photo luminance quantum yield (PLQY), $CsPbBr_3$ perovskite draws substantial attentions for application in LEDs with unique emission characteristics, e.g. narrow emission spectrum and low turn-on voltage [20, 21]. $CsPbBr_3$ perovskite with simultaneous excellent light harvesting and light emitting properties make it a very suitable candidate for use in multi-functional optoelectronics.

In this work, we report our efforts to develop high performing $CsPbBr_3$ perovskite-based bi-functional diodes. The $CsPbBr_3$ perovskite functional layer in the bi-functional diode serves as a light emission layer when the diode is operated at a forward bias, and it becomes a light detection layer while the diode is operated under a reverse bias. The excellent optoelectronic properties of the $CsPbBr_3$ perovskite layer, such as saturated green light emission and good light absorption in the ultraviolet (UV)-visible light wavelength range, enable the realization of the electroluminescence (EL) and photo-response dual function in one device. The EL characteristics, functioning as a LED, and photo-response properties, acting as a PD, of the bi-functional diode can be realized by controlling the polarity of the external biases. The unique EL and photo-response dual-function in one identical device has the advantage in reducing the complexity of device configuration, which often involves the use of tandem structure, and thereby simplifying the fabrication procedures. It was also found that the bi-functional diodes exhibit very fast transient EL and transient photo-response characteristics, which are a prerequisite for application in optical communication. A visible light communication system operated at 520 nm was demonstrated utilizing two identical bi-functional diodes, one functioned as the signal generator and the other acted as the signal receiver. The outcomes of the work are very encouraging. It is anticipated that the inorganic halide perovskite bi-functional diodes can be a commercial viable technology for applications in, e.g. Internet of Things, smart lighting, indoor visible light and under-water communication etc.

## 2 Methods

The $CsPbBr_3$ precursor was prepared in a non-stoichiometric manner with excess CsBr [9, 20]. 0.18 M $PbBr_2$ (Sigma Aldrich) and 0.324 M CsBr (Sigma Aldrich) were dissolved in dimethyl sulfoxide (Sigma Aldrich) and kept stirring before use. All chemicals are used as received. 180 nm thick pre-patterned indium tin oxide (ITO)-coated glass substrates, with a sheet resistance of 100 ohm per square, were cleaned by ultra-sonication sequentially with diluted detergent, deionized water, acetone and isopropyl alcohol each for 15 min. After drying in oven, the ITO/glass substrates were exposed to the UV-Ozone for 10 min to remove the residual chemicals on ITO surface. The UV-Ozone treatment also helps to improve the surface hydrophilicity assisting in the deposition of the Poly(3,4-ethylenedioxythiophene)-poly(styrenesulfonate) (PEDOT:PSS) hole transporting layer (HTL) in air. A 40 nm thick PEDOT:PSS HTL was optimized by controlling the spin coating conditions. The substrates with PEDOT:PSS thin film were annealed at 140°C for 10 min to remove the residual water and then transferred into glove box with oxygen and $H_2O$ levels below 0.1 ppm. Afterwards, the $CsPbBr_3$ thin film was grown on the surface of the PEDOT:PSS HTL using two different approaches, e.g. (1) drop-spin method and (2) spin-drop method. In the drop-spin method, 80 µl precursor was dropped to the surface of PEDOT:PSS HTL and the substrate rotation was started only after the perovskite precursor solution was spread evenly across the substrate. While in the spin-drop method, substrate rotation occurred prior to the drop of the 80 µl precursor solution. The thickness of the $CsPbBr_3$ layers was controlled by the rotation speed in the spin-coating process, e.g. the $CsPbBr_3$ thicknesses of 26 nm, 30 nm and 36 nm were prepared using different rotation speeds of 3500 rpm, 3000 rpm, and 2500 rpm for 60 s, respectively. The $CsPbBr_3$ thin films were annealed at 70°C for 10 min in the glove box, the samples were transferred to the vacuum chamber for deposition of 100 nm thick 2,2′,2″-(1,3,5-Benzinetriyl)-tris(1-phenyl-1-H-benzimidazole) (TPBi) electron transportation layer (ETL), 1 nm LiF electron injection layer (EIL) and 100 nm thick Al electrode, prepared by thermal evaporation. The devices were encapsulated in the glove box before the measurements. The active area of the device is ~0.1 $cm^2$.

The UV-visible absorption spectra of the $CsPbBr_3$ active layers were recorded using a HP 8453 spectrophotometer. The morphological characteristics of the thin film were investigated using scanning electron microscope (SEM) by a LEO 1530 system. The crystallinity of the $CsPbBr_3$ active layer was measured by X-ray Diffraction (XRD) technique. The photoluminescence (PL) properties of the thin film were characterized using a He-Cd laser operated at 325 nm as the activation light. The luminance–current density–voltage (*L–J–V*) characteristics of the bi-functional diodes were characterized using a luminance colorimeter, an electro meter and control software. Two LED (Zolix) light sources with different peak EL wavelengths of 365 nm and 450 nm were used for measuring the photo-response behavior of the bi-functional diodes. The transient EL of

the bi-functional diodes was detected using a commercial Si photodiode (Thorlabs) and recorded by an oscilloscope (Tektronix). The transient photo-response of the PDs was recorded on an oscilloscope under pulsed blue light (450 nm). All the optoelectronic measurements were conducted in ambient.

## 3 Results and discussion

In inorganic halide perovskite $CsBbBr_3$-based optoelectronic devices, huge attention has been devoted to the synthesis of $CsBbBr_3$ quantum dots (QDs) [21, 22, 25–27] for high performance, e.g. PLQY [27, 28]. However, the synthesis procedures usually include complex passivation of the QD surfaces which causes injection barriers due to the surface ligands [29]. Thin film $CsPbBr_3$ perovskite based devices are becoming a promising choice for functional optoelectronics [30–33] due to the ease of fabrication using costless techniques like spin coating and spray coating. The morphology of the $CsPbBr_3$ emission layer plays a critical role in achieving high luminous efficiency of $CsPbBr_3$-based LEDs [34, 35].

In this work, it is found that the coating method of the $CsPbBr_3$ layer has a huge impact on the thin film morphology. The intrinsic fast crystallization of the $CsPbBr_3$ perovskite tends to form different morphological features depending on the spin coating methods. In the drop-spin method where the substrate rotation was set after the casting of the precursor, the fast crystallization of $CsPbBr_3$ tends to form ring-like features during the slow free spread as schematically shown in Figure 1A. The left insert in Figure 1A is a photo taken for $CsPbBr_3$ thin film on ITO/HTL with clear ring like features under 350 nm UV light. The LEDs based on these ring-featured thin films also exhibit un-uniform light emission as shown in the right insert in Figure 1A. The clear ring features observable to the naked eye in the $CsPbBr_3$ thin film is attributed to the fast crystallization of the $CsPbBr_3$ material during the slow precursor spread. The ring-like feature of the film is formed due to the distribution of the spatially varying layer thickness. The corresponding profile of the layer thickness across the $CsPbBr_3$ surface is clearly seen in the step profiler measurement. Figure S1 (in Supporting Information) shows the photograph taken for the measurement using the step-profiler and the direction of the line scanning in the measurement. The line profile of the ring-like surface was given in Figure S2. Clear height peaks can be seen in the profile of the film thickness along the scan direction, corresponding to the position of the "ring" feature in the film. The schematic diagram illustrating the formation of the ring-like features is shown in Figure S3. The precursor was casted on the substrate and spread freely in the film formation. During this period, the ring-like features were formed due to the fast crystallization of the $CsPbBr_3$ film. To deal with this inhomogeneous thin film formation, a spin-drop method was introduced where the precursor was casted on a rotating substrate. This method provides a centrifugal force during the precursor spread as schematically illustrated in Figure 1B. As a consequence, a highly repeatable uniform $CsPbBr_3$ thin film was obtained as the photograph shown in left insert of Figure 1B under UV light. The uniform surface profile of the $CsPbBr_3$ thin film is presented in Figure S4, without any height peaks that were seen in the ring-like films. The LED with the uniform $CsPbBr_3$ thin film shows homogenous light emission as the photo shown in right insert of Figure 1B. The centrifugal force provided by the rotating substrate assists the precursor spread which is responsible for the formation of highly reproducible and uniform $CsPbBr_3$ emission layer.

The characteristics of the uniform $CsPbBr_3$ thin films were investigated by SEM and XRD techniques. The top view SEM image of $CsPbBr_3$ thin film is shown in Figure 2A. Uniformly distributed $CsPbBr_3$ crystals with relative small sized polycrystalline features were obtained [20, 36]. The spinodal decomposition mechanism is likely to play a role in the formation of the $CsPbBr_3$ thin film, leading to a finely dispersed microstructure, as shown in Figure 2A. The uniformly distributed small $CsPbBr_3$ crystal grains have the advantages for light emission. The XRD pattern shown in Figure 2B, exhibits three typical diffraction peaks at 15.2, 21.5, and 30.4 degree, which could be assigned to the (100), (110) and (220) planes of the $CsPbBr_3$ crystal, identifying the formation of

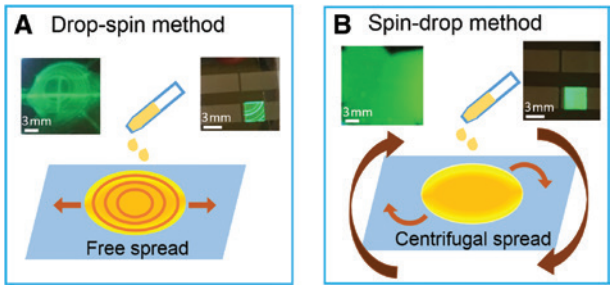


**Figure 1:** Schematic diagrams illustrating the quality of the $CsPbBr_3$ thin films prepared by (A) drop-spin and (B) spin-drop methods. The inserts in (A): the photo pictures taken for the $CsPbBr_3$ thin film grown on PEDOT:PSS/ITO exposed under UV light (left) and a bi-functional diode emitting light at 3 V (right). The inserts in (B): the photo pictures taken for the $CsPbBr_3$ thin film grown on PEDOT:PSS/ITO exposed under UV light (left) and a bi-functional diode emitting a uniform light at 3 V (right).

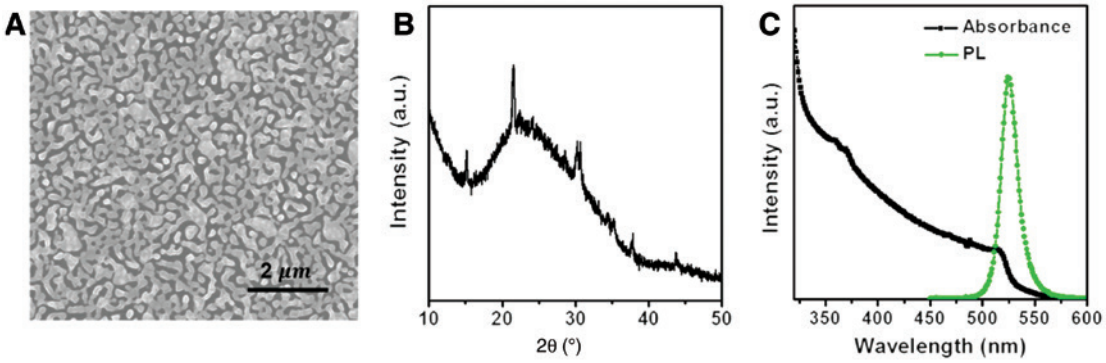


**Figure 2:** $CsPbBr_3$ perovskite thin film characteristics.
(A) Top view SEM image, and (B) XRD spectrum measured for the $CsPbBr_3$ perovskite thin film deposited on the PEDOT:PSS /ITO substrates, and (C) absorption and PL spectra measured for the $CsPbBr_3$ perovskite thin film deposited on the quartz substrates.

orthorhombic structure of the crystal [17, 33]. The absorbance and static PL spectra of $CsPbBr_3$ thin film are illustrated in Figure 2C. Clearly, the maxima of the PL signal is located near the absorption edge with an insignificant difference indicating the PL emission of $CsPbBr_3$ originates from direct recombination of charges across the band edge of $CsPbBr_3$ [20]. The absorption spectrum shows $CsPbBr_3$ thin film is capable of absorbing photons with energy higher than its bandgap of ~2.3 eV [19, 36], such that it is a good light absorber for UV and portion of visible light. The PL spectrum of $CsPbBr_3$ thin film is very narrow with a FWHM of ~20 nm, indicating $CsPbBr_3$ perovskite is an appealing material for saturated light emission. These unique properties featuring simultaneously excellent light absorption and emission suggest that $CsPbBr_3$ perovskite is a versatile material for multi-functional optoelectronic devices.

The diode consisting a $CsPbBr_3$ thin film as the active layer with a configuration of ITO/PEDOT:PSS/$CsPbBr_3$/TPBi/LiF/Al was fabricated and characterized. The $CsPbBr_3$ layer was sandwiched between a HTL PEDOT:PSS and an ETL TPBi as schematically shown in Figure 3A, which is a typical structure in $CsPbBr_3$ perovskite based LEDs [30, 37, 38]. The diode possesses bi-functionality by controlling the bias polarity as depicted in Figure 3A. With forward bias, the diode works in the LED mode where holes and electrons are injected to the $CsPbBr_3$ emissive layer as shown in Figure 3B, resulting in EL. While with reverse bias, the diode function as a PD in which photo generated holes and electrons are formed and then collected by respective electrodes driven by the external electric field. The schematic working mechanism is shown in Figure 3C. This EL and photo-response bi-functionality in one device takes advantage of the versatile properties of the $CsPbBr_3$ perovskite active layer.

The EL properties of the bi-functional diodes were firstly investigated and the performances were optimized

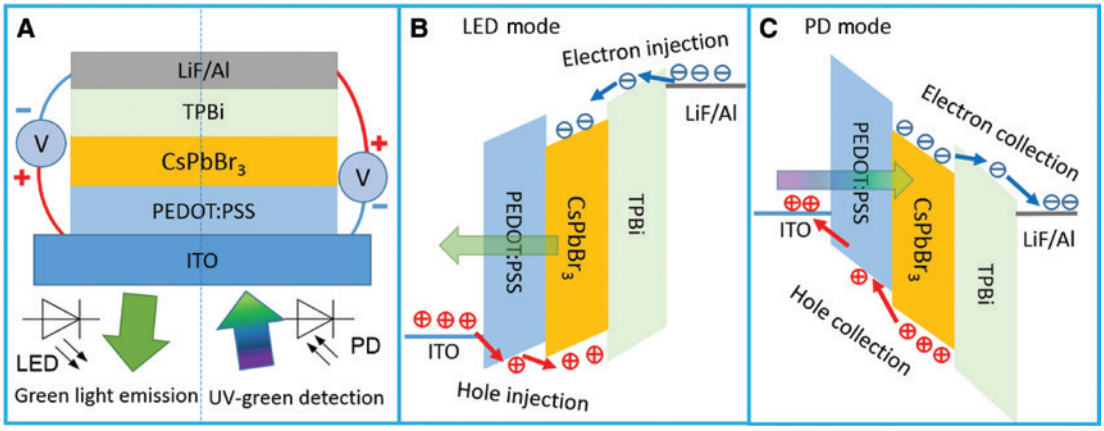


**Figure 3:** Schematics of the working mechanism of the bi-functional diodes.
(A) Schematic cross-sectional view of the bi-functional diode and its EL and photo-response dual-function. Schematic diagrams illustrating (B) charge injection for light-emitting process when the bi-functional diode is operated at a forward bias and (C) charge extraction for light detection when it is operated at a reverse bias.

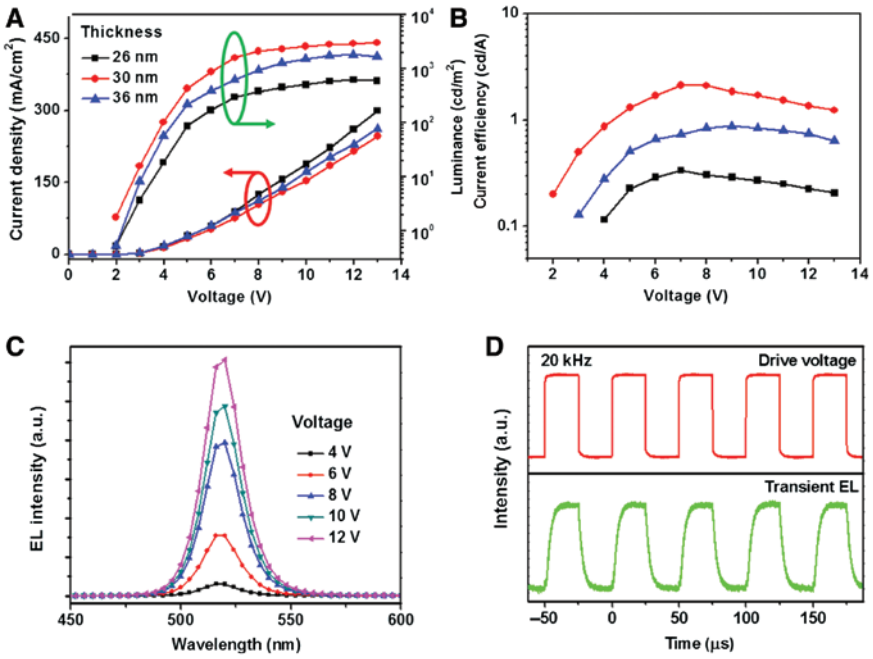


**Figure 4:** Electroluminescence characteristics of the bi-functional diodes.
(A) *J–L–V* characteristics and (B) current efficiency measured for the bi-functional diodes with different active layer thicknesses of 26 nm, 30 nm and 36 nm. (C) Typical EL spectra measured for the bi-functional diode at different forward biases. (D) The transient EL characteristics of the bi-functional diode operated by a 5 V 20 kHz-modulated power source. The profile of the 20 kHz-modulated bias also is plotted for comparison.

by controlling the thickness of $CsPbBr_3$ perovskite layer. The *L–J–V* characteristics were shown in Figure 4A. With increasing the forward bias, the current density as well as the luminance of all LEDs increases. And all three devices with different active layer thickness exhibit a low turn-on voltage of ~2V. The ultra-low turn-on voltage even lower than the band gap of the material (~2.3 eV) suggests an extremely efficient charge injection from charge transporting layers to the active layer [36]. The 30 nm-thick $CsPbBr_3$ perovskite active layer based LED shows relatively higher luminescence as compared to the other two devices with the thickness (26 and 36 nm) of $CsPbBr_3$ layer, achieving a maximum luminance of 3035 cd/cm$^2$ at a forward bias of 13 V. The current efficiency of the three LEDs as a function of active layer thickness and bias voltage are given in Figure 4B. The LED with a thickness of 30 nm for active layer achieved higher current efficiency due to an enhanced EL performance. All LEDs exhibit a voltage independent emission spectrum.

The EL spectra of the LED with 30 nm-thick $CsPbBr_3$ perovskite layer were plotted in Figure 4C as a function of bias voltage. Identical EL peak were observed regardless the bias voltage. The EL spectra were also in good agreement with the PL characteristics. The transient EL performance of the diodes in the LED mode was also investigated. A function generator was employed serving as the power supply. The transient EL of the diode was detected using a commercial Si photodiode and recorded by oscilloscope. In Figure 4D, the transient EL were compared to the corresponding driving signal of the functional generator at a frequency of 20 kHz. The rise and fall time of EL was measured to be ~6 μS suggesting the LEDs are potentially suitable for transient light generators in high speed visible communication systems.

The PD characteristics of the bi-functional diode were then carried out. The $CsPbBr_3$ perovskite active layer was controlled to be 30 nm. In Figure 5A, the external quantum efficiency (*EQE*) and photoresponsivity (*R*) of the bi-functional diode as a function of wavelength operated at 0 V were presented. The photoresponsivity defined as $R=I_{photo}/P_{in}$, where $I_{photo}$ is the photocurrent and $P_{in}$ is the incident light power, has a close relationship with *EQE* in the form of $R=EQE/hv$, where *R* is in A/W and *hv* is the incident photon energy in eV. These results indicate the diode can be operated in a self-powered mode where photo-generated charges could be collected under the built-in potential. The *EQE* of 7% and photoresponsivity of 20 mA/W were obtained at 350 nm. The collection efficiency of the photo-generated charges can be largely improved by applying a reverse bias on the PD. The photo-response of the bi-functional diodes under reverse bias was measured under light illumination of 365 nm and 450 nm. The current-voltage characteristics of the diodes under 365 nm and 450 nm light illumination were presented in Figure 5B. The bi-functional diode shows

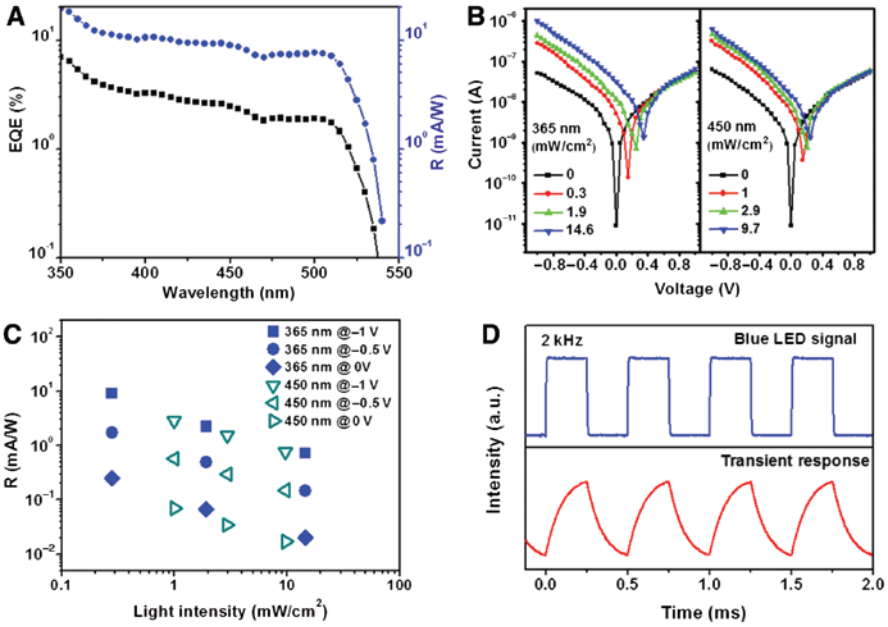


**Figure 5:** Photo-response properties of the bi-functional diodes.
(A) *EQE* and corresponding photoresponsivity of the bi-functional diode at 0 V bias, (B) the photo current–voltage characteristics measured for the bi-functional diodes using two LED sources with different peak EL wavelengths of 365 and 450 nm under different light intensities. (C) The photoresponsivity–light intensity characteristics measured for the bi-functional diode operated at different reverse biases using two LED light sources. (D) The transient photo-response of the bi-functional diode operated at 0 V under a 2 kHz-modulated 450 nm blue light LED source.

good photo-response both under 365 nm and 450 nm. With the increase of the reverse bias, the photo current increases due to enhanced charge collection with the help of external electrical field. In Figure 5C, the extracted photoresponsivity of the diodes as a function of reverse bias and light intensity were summarized. The photoresponsivity of the diodes show a light intensity dependent manner similar to that of the commercialized photodetectors. At a higher reverse bias, the photoresponsivity enhances due to improved collection efficiency of the photo-generated charges. Compared to the results of the $CsPbBr_3$-based photodetectors [20, 21], the devices benefit from a lower driving voltage which is potentially attractive for low-power portable and wearable applications. The transient photo-response of the bi-functional diode was estimated by applying a series of blue light signals to the device and recording the photo current signals. The profile of the blue light signals and the photo-response of the diode operated at 0 V are given in Figure 5D. According to the transient photo-response profile, the rise and fall time of the diode were estimated to be ~160 and ~170 μS. The transient photo-response was fast as compared to that of the reported $CsPbBr_3$ based detectors [22, 23].

The fast transient EL and photo-response of the bi-functional diodes indicate their potential for application in optical communication systems. It is interesting that the bi-functional diode in PD mode could response well to the light emitted by another identical diode in LED mode. This is due to the overlap of the light emission spectra and absorption profile as shown in Figure 2C. A visible light communication system using the bi-functional diode simultaneously as signal generator and receiver was experimentally demonstrated. The schematic set up was shown in Figure 6A. The LED mode diode was driven by a function generator while another identical diode operated in the PD mode was connected to the oscilloscope. As shown in Figure 6B–D, the light signal from the LED mode diode and the photo-response signal from the PD mode diode are compared at different frequencies. The visible communication system operated well at frequencies from 500 Hz to 2 kHz. It is noteworthy that the system operating speed is limited by the PD mode diode due to a relatively slower transient photo-response as compared to the transient EL.

This is the first demonstration of a visible light communication system using two identical $CsPbBr_3$ based diodes as signal generator and receiver at the same time. The bi-functional diodes with ability in broadband light detection from UV to visible range and light emission at green light are promising in multi-functional electronic applications.

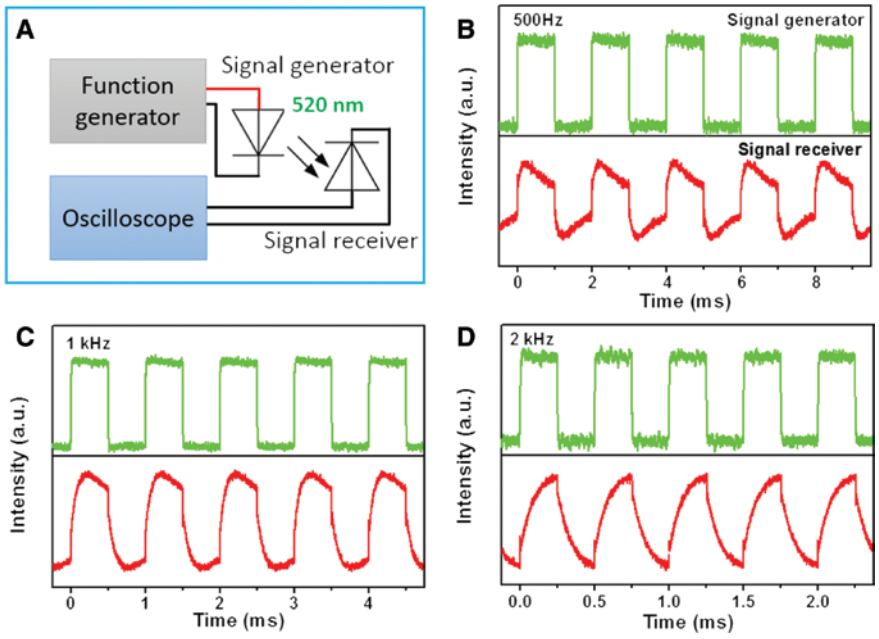


**Figure 6:** The demonstration of the visible light communication system.
(A) The schematic diagram illustrating the use of two identical bi-functional diodes for application in high speed visible light communication, one performed as a signal generator and another diode, placed 0.5 m away, acted as a signal receiver. The modulated EL emission and the corresponding photo-response of a pair of the bi-functional diodes, performing the visible light communication capability, at different frequencies of (B) 500 Hz, (C) 1 kHz, and (D) 2 kHz, were clearly manifested. The diode that functioned as the signal generator was operated at a forward bias of 5 V, and the one acted as the receiver was operated at 0 V.

## 4 Conclusions

In this work, the formation of highly reproducible and uniform $CsPbBr_3$ perovskite thin film layer was investigated. Our findings reveal that a uniform $CsPbBr_3$ perovskite thin film can be readily achieved by applying a centrifugal force during the spread of the precursor. This method avoids the ring-like inhomogeneous film morphology. The resulting highly uniform $CsPbBr_3$ perovskite thin films with high reproducibility were then utilized as the active layer in the diode configuration. These diodes not only emit green light with forward bias, but also exhibit UV-visible broadband light detection abilities by applying reverse bias. The bi-functionality of the diode originates from the outstanding optoelectronic features of the $CsPbBr_3$ perovskite active material. With fast transient EL and photo-response properties of the bi-functional diodes, a visible light communication system was demonstrated. The system employed two structurally identical bi-functional diodes, one operated in the LED mode as the signal generator and the other in the PD mode as signal receiver, respectively. This green light communication system is potentially useful in the under-water communication systems due to less absorption of sea water at this wavelength.

**Acknowledgment:** This work was financially supported by the Research Grants Council of Hong Kong Special Administrative Region, China, General Research Fund (GRF/12302817), Hong Kong Baptist University Inter-institutional Collaborative Research Scheme (RC-ICRS/15-16/04), and National Natural Scientific Foundation of China (61705156).

## References

[1] Wang XZ, Tam HL, Yong KS, Chen ZK, Zhu FR. High performance optoelectronic device based on semitransparent organic photovoltaic cell integrated with organic light-emitting diode. Org Electron 2011;12:1429–33.
[2] Ho YH, Liang H, Liu SW, Tian WC, Chen FC, Wei PK. Efficiency improvement of organic bifunctional devices by applying omni-directional antireflection nanopillars. RSC Adv 2014;4:9588–93.
[3] Ali F, Periasamy N, Patankar MP, Narasimhan KL. Integrated organic blue LED and visible-blind UV photodetector. J Phys Chem C 2011;115:2462–9.
[4] Wang H, Zhou J, Wang X, Lu Z, Yu J. High performance organic integrated device with ultraviolet photodetective and electroluminescent properties consisting of a charge-transfer-featured naphthalimide derivative. Appl Phys Lett 2014;105:122.
[5] Wang X, Zhou D, Huang J, Yu J. High performance organic ultraviolet photodetector with efficient electroluminescence realized

by a thermally activated delayed fluorescence emitter. Appl Phys Lett 2015;107:73.
[6] Miao Y, Wang K, Zhao B, et al. High-efficiency/CRI/color stability warm white organic light-emitting diodes by incorporating ultrathin phosphorescence layers in a blue fluorescence layer. Nanophotonics 2018;7:295–304.
[7] Tao P, Miao Y, Wang H, Xu B, Zhao Q. High-performance organic electroluminescence: Design from organic light-emitting materials to devices. Chem Rec 2018; DOI: 10.1002/tcr.201800139.
[8] Miao Y, Tao P, Wang K, et al. Highly efficient red and white organic light-emitting diodes with external quantum efficiency beyond 20% by employing pyridylimidazole-based metallophosphors. ACS Appl Mater Interfaces 2017;9:37873 – 82.
[9] Liu M, Johnston MB, Snaith HJ. Efficient planar heterojunction perovskite solar cells by vapour deposition. Nature 2013;501:395–8.
[10] Zhou H, Chen Q, Li G, et al. Interface engineering of highly efficient perovskite solar cells. Science 2014;345:542–6.
[11] Jeon NJ, Noh JH, Kim YC, Yang WS, Ryu S, Seok SI. Solvent engineering for high-performance inorganic-organic hybrid perovskite solar cells. Nat Mater 2014;13:897–903.
[12] Green MA, Ho-Baillie A, Snaith HJ. The emergence of perovskite solar cells. Nat Photonics 2014;8:506–14.
[13] Tan ZK, Moghaddam RS, Lai ML, et al. Bright light-emitting diodes based on organometal halide perovskite. Nat Nanotechnol 2014;9:687–92.
[14] Cho H, Jeong SH, Park MH, et al. Overcoming the electroluminescence efficiency limitations of perovskite light-emitting diodes. Science 2015;350:1222–5.
[15] Jin FM, Zhao B, Chu B, et al. Morphology control towards bright and stable inorganic halide perovskite light-emitting diodes. J Mater Chem C 2018;6:1573–8.
[16] Li N, Lau YS, Xiao Z, Ding LM, Zhu FR. NIR to visible light upconversion devices comprising an NIR charge generation layer and a Perovskite emitter. Adv Opt Mater 2018; DOI: 10.1002/adom.201801084.
[17] Sutton RJ, Eperon GE, Miranda L, et al. Bandgap-tunable cesium lead halide perovskites with high thermal stability for efficient solar cells. Adv Energy Mater 2016;6:1502458.
[18] Kulbak M, Gupta S, Kedem N, et al. Cesium enhances long-term stability of lead bromide perovskite-based solar cells. J Phys Chem Lett 2016;7:167–72.
[19] Liang J, Wang C, Wang Y, et al. All-inorganic perovskite solar cells. J Am Chem Soc 2016;138:15829–32.
[20] Yantara N, Bhaumik S, Yan F, et al. Inorganic halide perovskites for efficient light-emitting diodes. J Phys Chem Lett 2015;6:4360–4.
[21] Li X, Wu Y, Zhang S, et al. $CsPbX_3$ quantum dots for lighting and displays: room-temperature synthesis, photoluminescence superiorities, underlying origins and white light-emitting diodes. Adv Funct Mater 2016;26:2435–45.
[22] Ramasamy P, Lim DH, Kim B, Lee SH, Lee MS, Lee JS. All-inorganic cesium lead halide perovskite nanocrystals for photodetector applications. Chem Commun 2016;52:2067–70.
[23] Liu H, Zhang X, Zhang L, et al. A high-performance photodetector based on an inorganic perovskite-ZnO heterostructure. J Mater Chem C 2017;5:6115–22.
[24] Li X, Yu D, Cao F, et al. Healing All-inorganic perovskite films via recyclable dissolution-recyrstallization for compact and smooth carrier channels of optoelectronic devices with high stability. Adv Funct Mater 2016;26:5903–12.
[25] Swarnkar A, Chulliyil R, Ravi VK, Irfanullah M, Chowdhury A, Nag A. Colloidal $CsPbBr_3$ perovskite nanocrystals: luminescence beyond traditional quantum dots. Angew Chemie 2015;54:15424–8.
[26] Li G, Rivarola FWR, Davis NJKL, et al. Highly efficient perovskite nanocrystal light-emitting diodes enabled by a universal crosslinking method. Adv Mater 2016;28:3528–34.
[27] Bekenstein Y, Koscher BA, Eaton SW, Yang P, Alivisatos AP. Highly luminescent colloidal nanoplates of perovskite cesium lead halide and their oriented assemblies. J Am Chem Soc 2015;137:16008–11.
[28] Pan J, Sarmah SP, Murali B, et al. Air-stable surface-passivated perovskite quantum dots for ultra-robust, single- and two-photon-induced amplified spontaneous emission. J Phys Chem Lett 2015;6:5027–33.
[29] Kumawat NK, Gupta D, Kabra D. Recent advances in metal halide-based perovskite light-emitting diodes. Energy Technol 2017;5:1734–49.
[30] Zhang X, Wang W, Xu B, et al. Thin film perovskite light-emitting diode based on $CsPbBr_3$ powders and interfacial engineering. Nano Energy 2017;37:40–5.
[31] Li Y, Shi ZF, Li S, et al. High-performance perovskite photodetectors based on solution-processed all-inorganic $CsPbBr_3$ thin films. J Mater Chem C 2017;5:8355–60.
[32] Wu C, Zou Y, Wu T, et al. Improved performance and stability of all-Inorganic perovskite light-emitting dodes by antisolvent vapor treatment. Adv Funct Mater 2017;27:1700338.
[33] Zhang L, Yang X, Jiang Q, et al. Ultra-bright and highly efficient inorganic based perovskite light-emitting diodes. Nat Commun 2017;8:15640.
[34] Jin F, Zhao B, Chu B, et al. Morphology control towards bright and stable inorganic halide perovskite light-emitting diodes. J Mater Chem C 2018;6:1573–8.
[35] Salim T, Sun S, Abe Y, Krishna A, Grimsdale AC, Lam YM. Perovskite-based solar cells: impact of morphology and device architecture on device performance. J Mater Chem A 2015;3:8943–69.
[36] Ng YF, Jamaludin NF, Yantara N, et al. Rapid crystallization of all-Inorganic $CsPbBr_3$ perovskite for high-brightness light-emitting diodes. ACS Omega 2017;2:2757–64.
[37] Zhang X, Xu B, Zhang J, et al. All-Inorganic perovskite nanocrystals for high-efficiency light emitting diodes: dual-phase $CsPbBr_3$-$CsPb_2Br_5$ composites. Adv Funct Mater 2016;26:4595–600.
[38] Ling Y, Tian Y, Wang X, et al. Enhanced optical and electrical properties of polymer-assisted all-Inorganic perovskites for light-emitting diodes. Adv Mater 2016;28:8983–9.

**Supplementary Material:** The online version of this article offers supplementary material (https://doi.org/10.1515/nanoph-2018-0149).